Journal of Computational Physics 227 (2008) 8841–8854

Contents lists available at ScienceDirect

Journal of Computational Physics

journal homepage: www.elsevier.com/locate/jcp

High-order mimetic finite difference method for diffusion problems on polygonal meshes

Vitaliy Gyrya [a,*], Konstantin Lipnikov [b]

[a] The Pennsylvania State University, Department of Mathematics, University Park, PA 16802, USA
[b] Los Alamos National Laboratory, MS B284, Los Alamos, NM 87545, USA

ARTICLE INFO

Article history:
Received 30 October 2007
Received in revised form 20 June 2008
Accepted 23 June 2008
Available online 3 July 2008

Keywords:
Diffusion equation
Locally conservative method
Mimetic discretization
High-order method
Polygonal mesh

ABSTRACT

The mimetic finite difference (MFD) methods mimic important properties of physical and mathematical models. As a result, conservation laws, solution symmetries, and the fundamental identities of the vector and tensor calculus are held for discrete models. The MFD methods retain these attractive properties for full tensor coefficients and arbitrary polygonal meshes which may include non-convex and degenerate elements. The existing MFD methods for solving diffusion-type problems are second-order accurate for the conservative variable (temperature, pressure, energy, etc.) and only first-order accurate for its flux. We developed new high-order MFD methods which are second-order accurate for both scalar and vector variables. The second-order convergence rates are demonstrated with a few numerical examples on randomly perturbed quadrilateral and polygonal meshes.

Published by Elsevier Inc.

1. Introduction

Modeling with arbitrary polygonal and polyhedral meshes has a number of advantages. In modeling of subsurface flows such meshes allow to describe accurately small, detailed structures, such as tilted layers, pinch-outs and irregular inclusions. The polygonal and polyhedral meshes cover the space more efficiently than simplicial meshes which eventually reduces the number of discrete unknowns. The locally refined meshes with hanging nodes are used frequently to improve resolution in the regions of interest, such as moving fluid fronts and sharp solution variations. Such meshes are particular examples of polygonal and polyhedral meshes with degenerate elements. Here we develop new mimetic finite difference (MFD) methods for solving a linear diffusion problem on arbitrary polygonal meshes. The methods are developed and tested in two dimensions, however, the underlying ideas may be extended to polyhedral meshes with planar mesh faces.

The MFD methods combine flexibility of finite volume methods with analytical power of finite element methods. Their success in different applications [1,2,5,7,11,14] is due to *mimicking* essential properties of the continuum models, such as conservation laws, solution symmetry and positivity, and the fundamental identities and theorems of vector and tensor calculus. The MFD methods retain these attractive properties in the case of full tensor coefficients.

For the linear diffusion problem, the MFD methods *mimic* the Gauss divergence theorem, which results in locally conservative discretizations. These MFD methods, also, preserve symmetry between the gradient and divergence operators and the null spaces of these operators. The recently developed MFD methods (see [5,6] and references therein) are the low-order discretization methods. They provide the second-order convergence rate for the conservative variable (temperature, pressure, energy, etc.), and only the first-order convergence rate for its flux. More accurate flux resolution makes significant

* Corresponding author. Tel.: +1 973 865 1226.
E-mail addresses: gyrya@math.psu.edu (V. Gyrya), lipnikov@lanl.gov (K. Lipnikov).

0021-9991/$ - see front matter Published by Elsevier Inc.
doi:10.1016/j.jcp.2008.06.028

impact on evolution of physical systems [18]. We developed new MFD methods that are *second-order accurate for the flux variable*.

There are a few fundamentally different approaches to increasing accuracy of discretization methods. Finite volume and finite difference methods increase stencils of discrete operators which impose severe restrictions on mesh smoothness. To resolve this issue, high-order finite difference methods on non-uniform meshes were developed in [8,9] using mimetic ideas. However, these methods are limited to smooth quadrilateral meshes and lose accuracy on rough meshes. The finite element and spectral element methods increase the number of unknowns inside each element [10] but impose severe restrictions on the shape of admissible mesh elements. Other approaches use Padé-type approximations and are not practical for general meshes. Interesting blending of finite volume and finite element ideas in [17] resulted in new high-order finite volume methods on simplicial meshes. The high-order MFD methods proposed in this article blend ideas of finite element and recently developed low-order MFD methods [2,6]. They use the same discrete unknowns for the scalar variable as the low-order MFD methods and double the number of flux unknowns; the zeroth and first-order moments of the normal flux are defined on mesh edges. In case of triangular meshes, the distinction between the low-order and high-order MFD methods resembles that of the low-order Raviart–Thomas (RT_0) and Brezzi–Douglas–Marini (BDM_1) finite element methods [3].

Here we present two new high-order MFD methods. The development of the *first* high-order MFD method was inspired in part by ideas of low-order Kuznetsov–Repin finite element methods [12,13]. To construct an inner product in the space of discrete fluxes, we divide a polygon into triangles and use the existing formula for exact integration of linear fluxes on a triangle. The auxiliary triangular partition introduces additional flux unknowns on interior edges. Half of these unknowns, 0th moments of the normal flux, are eliminated using the Kuznetsov–Repin approach. The remaining unknowns are eliminated by mimicking integral identities for particular spaces of vector-functions. The method is useful for problems where the flux has to be recovered at some points inside polygonal elements (e.g. problems of reactive transport in porous media, compressible flows).

The development of the *second* high-order MFD method was inspired in part by the methods developed in [2,5,6]. Contribution of each polygonal element to the inner product matrix is calculated using only the boundary data (normals to polygon edges, length of edges, and quadrature rules for edge integrals). Since, no auxiliary triangular partition is required, the proposed method can be applied to meshes with degenerate polygons, which appear in adaptive mesh refinement (AMR) methods, and non-convex polygons, which appear in moving mesh methods. The method results in a family of discretization schemes (e.g. one parameter for every triangle and three parameters for every quadrilateral). In case of triangular meshes, this family contains the scheme arising from the BDM_1 finite element method [3, Chapter III]. In numerical experiments, we use the simplest choice for these parameters.

The paper outline is as follows: in Section 2, we present the high-order MFD method. In Section 3, we describe the inner product in the space of discrete fluxes. In Section 4, convergence of the method is verified by numerical experiments on quadrilateral and polygonal meshes.

2. Mimetic finite difference methods

We consider the stationary heat conduction equation in a polygonal domain Ω:

$$-\mathrm{div}(\mathbb{K}\nabla u) = q \quad \text{in } \Omega, \tag{2.1}$$

where u is the temperature, $\mathbb{K}$ is the *full* conductivity tensor and q is the forcing term indicating the source of heat. In this article, we consider the Dirichlet boundary conditions

$$u = u_0 \quad \text{on } \partial\Omega. \tag{2.2}$$

Eq. (2.1) can be written as a system of two linear equations for the scalar unknown u and its flux $\vec{F}$:

$$\mathrm{div}\vec{F} = q, \quad \vec{F} = -\mathbb{K}\nabla u \quad \text{in } \Omega. \tag{2.3}$$

The first equation is the conservation of heat and the second one is the constitutive equation.

The success of the mimetic finite difference method is in *mimicking* important properties of continuum equations such as the Green formula,

$$\int_\Omega \mathbb{K}^{-1}(\mathbb{K}\nabla u)\cdot\vec{F}\,\mathrm{d}x = -\int_\Omega u\,\mathrm{div}\vec{F}\,\mathrm{d}x + \int_{\partial\Omega} u_0\vec{F}\cdot\vec{n}\,\mathrm{d}x, \tag{2.4}$$

which expresses the symmetry relationship between operators div and $\mathbb{K}\nabla$. Hereafter all functions are assumed to be sufficiently smooth, such that all integrals do exist.

A finite difference discretization of the system (2.3) requires a discretization for the scalar functions u, q, the vector function $\vec{F}$, and the differential operators $\mathbb{K}\nabla$, div. Among all possible discrete operators approximating $\mathbb{K}\nabla$ and div, the mimetic approach uses only operators which satisfy a discrete Green formula. This requires to discretize integrals in (2.4). We introduce the following notations (more details are provided later):

$$u, v, q \to \mathbf{u}, \mathbf{v}, \mathbf{q} \in Q^h, \tag{2.5}$$

$$\vec{F}, \vec{G} \to \mathbf{F}, \mathbf{G} \in X^h, \tag{2.6}$$

$$\mathrm{div} \to \mathcal{DIV}^h : X^h \to Q^h, \tag{2.7}$$

$$\mathbb{K}\nabla \to \mathcal{GRAD}^h : Q^h \to X^h, \tag{2.8}$$

$$\int_\Omega uv\,\mathrm{d}x + \int_{\partial\Omega} uv\,\mathrm{d}x \to [\mathbf{u}, \mathbf{v}]_Q \equiv \mathbf{u}^{\mathrm{T}}\mathbf{M}_Q\mathbf{v}, \tag{2.9}$$

$$\int_\Omega \vec{F}\cdot\mathbb{K}^{-1}\vec{G}\,\mathrm{d}x \to [\mathbf{F}, \mathbf{G}]_X \equiv \mathbf{F}^{\mathrm{T}}\mathbf{M}_X\mathbf{G}. \tag{2.10}$$

With these notations, the discrete analog of the system (2.3) is

$$\mathcal{DIV}^h\mathbf{F}_h = \mathbf{q}, \quad \mathbf{F}_h = -\mathcal{GRAD}^h\mathbf{u}_h. \tag{2.11}$$

2.1. The discretization of scalar and vector-functions

The MFD discretization of scalar and vector-functions is fairly standard for readers familiar with the high-order mixed finite element methods. We consider a partition $\mathcal{T}_h$ of the computational domain Ω into $\mathcal{N}_E$ polygonal elements:

$$\Omega = \bigcup_{i=1}^{\mathcal{N}_E} E_i.$$

Let h_i denote the diameter of polygon E_i and $h = \max_i h_i$ be the discretization parameter. The area of E is denoted by $|E|$. We also write $|e|$ for the length of the edge e. Finally, let $\mathcal{N}_e$ be the number of edges in the polygonal mesh, and $\mathcal{N}_{e,0}$ be the number of boundary edges.

In the high-order MFD methods, a scalar function v is represented (inside Ω) by its average values on mesh elements:

$$(\mathbf{v})_i = \frac{1}{|E_i|}\int_{E_i} v\,\mathrm{d}x, \quad 1 \leqslant i \leqslant \mathcal{N}_E, \tag{2.12}$$

where $(\mathbf{v})_i$ denotes the ith component of vector $\mathbf{v}$. On each boundary edge of $\partial\Omega$, the function v is represented by two numbers, the first two moments of v:

$$(\mathbf{v})_{\mathcal{N}_E+j} = \int_{e_j} v(s)\,\mathrm{d}s, \quad (\mathbf{v})_{\mathcal{N}_E+\mathcal{N}_{e,0}+j} = \int_{e_j} v(s)s\,\mathrm{d}s, \quad 1 \leqslant j \leqslant \mathcal{N}_{e,0}, \tag{2.13}$$

where s is the edge parametrization, $s \in [-1/2, 1/2]$. We assume that the edge is parameterized from the end-point with the lower index to the end-point with the higher index. The integrals in (2.13) are the 0th and 1st moments of v, respectively. Sometimes it will be convenient to write $(\mathbf{v})_{E_i}$ instead of $(\mathbf{v})_i$, $(\mathbf{v})^0_{e_j}$ instead of $(\mathbf{v})_{\mathcal{N}_E+j}$, and $(\mathbf{v})^1_{e_j}$ instead of $(\mathbf{v})_{\mathcal{N}_E+\mathcal{N}_{e,0}+j}$.

We denote by Q^h the space of all possible representations of scalar functions. The dimension of Q^h is equal to $\mathcal{N}_E + 2\mathcal{N}_{e,0}$. For a function v, we denote by $(v)^I$ a vector from Q^h whose components are defined by (2.12) and (2.13). Whenever no confusion may arise, we shall use (2.5); for instance, we shall write $\mathbf{v}$ instead of $(v)^I$.

Let $\vec{n}_e$ be the unit normal vector to edge e. We assume that for any boundary edge e vector $\vec{n}_e$ points in an outward direction for Ω. A vector-function $\vec{G}$ is represented by the 0th and 1st moments of $\vec{G}\cdot\vec{n}_e$ on mesh edges:

$$\{(\mathbf{G})^0_j,\ (\mathbf{G})^1_j\} = \left\{\int_{e_j}\vec{G}(s)\cdot\vec{n}_{e_j}\,\mathrm{d}s, \quad \int_{e_j}\vec{G}(s)\cdot\vec{n}_{e_j}s\,\mathrm{d}s\right\}, \tag{2.14}$$

where $j = 1, \ldots, \mathcal{N}_e$.

We denote by X^h the space of all possible representations of vector functions using only moments (2.14). The dimension of X^h is equals to $2\mathcal{N}_e$. For a vector-function $\vec{G}$, we denote by $(\vec{G})^I$ a vector in X^h whose components are moments (2.14). Whenever no confusion may arise, we shall use (2.6); for instance, we shall write $\mathbf{G}$ instead of $(\vec{G})^I$.

The degrees of freedom in the low-order MFD method include (2.12) and only the 0th moments in (2.13) and (2.14). It was shown in [4] that the low-order MFD method is second-order accurate for the scalar variable and first-order accurate for the flux variable. Additional degrees of freedom are required to build the high-order MFD method (see Fig. 1).

Remark 1. Another high-order MFD method can be developed by using different degrees of freedom for the flux $\vec{F}$. For example, we may use 0th moments of $\vec{F}\cdot\vec{n}_e$ on two half-edges of every mesh edge e.

2.2. The discretization of integrals

Let $[\mathbf{u}, \mathbf{v}]_Q$ denote the inner product in Q^h. It can also be viewed as a quadrature rule for the inner product of two scalar functions:

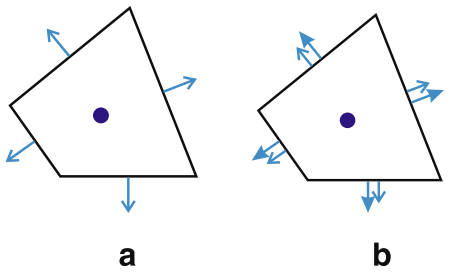

Fig. 1. Schematic illustration of degrees of freedom in the low-order (a) and high-order (b) MFD methods. The arrows represent flux unknowns. The solid circles represent temperature unknowns.

$$[\mathbf{u},\mathbf{v}]_Q \approx \int_\Omega uv\,dx + \sum_{e\in\partial\Omega}\int_e uv\,dx.$$

With the chosen degrees of freedom, the natural choice for the discrete inner product is

$$[\mathbf{u},\mathbf{v}]_Q = \sum_{E\in\mathcal{T}_h}|E|(\mathbf{u})_E(\mathbf{v})_E + \sum_{e\in\partial\Omega}\mathcal{Q}_e(\mathbf{u},\mathbf{v}), \tag{2.15}$$

where $\mathcal{Q}_e(\mathbf{u},\mathbf{v})$ is the quadrature rule for the edge integral. Since we have two degrees of freedom per mesh edge, we assume that this quadrature rule is exact for linear functions. Derivation of this quadrature rule is described in Appendix A.

Derivation of the inner product in X^h is less straightforward and will be discussed in Section 3. Let $\overline{\mathbb{K}}$ be a discontinuous piecewise constant approximation of tensor $\mathbb{K}$. We shall write $\overline{\mathbb{K}}_E$ for the value of $\overline{\mathbb{K}}$ on element E. We choose $\overline{\mathbb{K}}_E$ as the L^2-projection of $\mathbb{K}$ onto the space of piecewise constant tensors. Then, we write formally

$$[\mathbf{F},\mathbf{G}]_X = \sum_{E\in\mathcal{T}_h}[\mathbf{F},\mathbf{G}]_{X,E} \approx \sum_{E\in\mathcal{T}_h}\int_E \vec{F}\cdot\mathbb{K}^{-1}\vec{G}\,dx. \tag{2.16}$$

The formula for $[\cdot,\cdot]_{X,E}$ is derived in Section 3.

2.3. The discretization of operators

The discretization of the divergence operator div follows from the divergence theorem:

$$\int_E \mathrm{div}\vec{G}\,dx = \sum_{e\in\partial E}\int_e \vec{G}\cdot\vec{n}_E\,dx,$$

where $\vec{n}_E$ is the unit outward normal vector to ∂E. Using the central point quadrature rules, we get

$$(\mathcal{DIV}^{\mathrm{h}}\mathbf{G})_E = \frac{1}{|E|}\sum_{e\in\partial E}|e|(\mathbf{G})^0_e(\vec{n}_e\cdot\vec{n}_E). \tag{2.17}$$

Note that $\vec{n}_e\cdot\vec{n}_E$ is either 1 or -1 depending on the mutual orientation of normal vectors.

The discretization of the operator $\mathbb{K}\nabla$ follows from the discrete Green formula. But first, we define the *extended* discrete divergence operator:

$$\mathcal{D}^{\mathrm{h}}\mathbf{G} = \begin{cases} (\mathcal{DIV}^{\mathrm{h}}\mathbf{G})_E & \forall E\in\mathcal{T}_h,\\ (-(\mathbf{G})^0_e, -(\mathbf{G})^1_e)^{\mathrm{T}} & \forall e\in\partial\Omega. \end{cases}$$

Remark 2. In the case of homogeneous boundary conditions, $u_0 = 0$, the boundary term in the Green formula (2.4) disappears and there is no need to introduce the extended divergence operator.

We write the discrete Green formula by *mimicking* (2.4):

$$[\mathbf{G},\mathcal{GRAD}^{\mathrm{h}}\mathbf{v}]_X = -[\mathcal{D}^{\mathrm{h}}\mathbf{G},\mathbf{v}]_Q \quad \forall\mathbf{G}\in X^h \quad \forall\mathbf{v}\in Q^h. \tag{2.18}$$

Finally, let matrices $\mathbf{M}_X$ and $\mathbf{M}_Q$ represent inner products (2.15) and (2.16), respectively. Substituting this in (2.18), we get the explicit formula for the discrete gradient operator:

$$\mathcal{GRAD}^{\mathrm{h}} = -\mathbf{M}_X^{-1}(\mathcal{D}^{\mathrm{h}})^{\mathrm{T}}\mathbf{M}_Q. \tag{2.19}$$

Thus, the discrete gradient operator is negatively adjoint to the discrete extended divergence operator with respect to inner products in X^h and Q^h. Let Q_h^0 be the subspace of Q_h corresponding to constant functions. Formulas (2.12) and (2.13) give the following characterization of the space Q_h^0.

An element $\mathbf{v} \in Q_h$ belongs to the space Q_h^0 if and only if

$$(\mathbf{v})_i = (\mathbf{v})_1 \quad \text{for } i \leqslant \mathcal{N}_E + \mathcal{N}_{e,0}, \tag{2.20}$$

$$(\mathbf{v})_i = 0 \qquad \text{for } i > \mathcal{N}_E + \mathcal{N}_{e,0}. \tag{2.21}$$

Lemma 3. *Q_h^0 is the null space of the operator $\mathcal{GRAD}^{\mathrm{h}}$.*

Proof. We show that $\mathbf{v} \in Q_h$ is in the null space of the operator $\mathcal{GRAD}^{\mathrm{h}}$ if and only if (2.20) and (2.21) are satisfied. Since (2.20) and (2.21) hold only for elements of Q_h^0, this will complete the proof.

An element $\mathbf{v} \in Q_h$ is in the null space of $\mathcal{GRAD}^{\mathrm{h}}$ if and only if

$$[\mathbf{G}, \mathcal{GRAD}^{\mathrm{h}}\mathbf{v}]_X = -[\mathcal{D}^{\mathrm{h}}\mathbf{G}, \mathbf{v}]_Q = 0 \quad \forall \mathbf{G} \in X_h. \tag{2.22}$$

In particular, for (2.22) to hold it is necessary and sufficient that it holds for all $\widetilde{\mathbf{G}}$ that are the basis elements of X_h.

Let $\widetilde{\mathbf{G}} \in X_h$ be such that $(\widetilde{\mathbf{G}})^0_{e_k} = 1$ and all other components are zero. Consider the case when e_k is an interior edge shared by elements E_i and E_j. For this $\widetilde{\mathbf{G}}$ we rewrite (2.22), using definition (2.17) of the discrete divergence operator,

$$[\mathcal{D}^{\mathrm{h}}\widetilde{\mathbf{G}}, \mathbf{v}]_Q = (\vec{n}_{e_k} \cdot \vec{n}_{E_i})|e_k|((\mathbf{v})_{E_i} - (\mathbf{v})_{E_j}) = 0. \tag{2.23}$$

Since e_k is an arbitrary interior edge (2.23) implies that $(\mathbf{v})_{E_i} = (\mathbf{v})_1$.

Now we consider the case when e_k is a boundary edge that belongs to the element E_i. For this $\widetilde{\mathbf{G}}$ we rewrite (2.22), again, using definition (2.17)

$$[\mathcal{D}^{\mathrm{h}}\widetilde{\mathbf{G}}, \mathbf{v}]_Q = |e_k|((\mathbf{v})_{E_i} - (\mathbf{v})^0_{e_k}) = 0. \tag{2.24}$$

Since e_k is an arbitrary boundary edge (2.24) implies that $(\mathbf{v})^0_{e_k} = (\mathbf{v})_1$. Thus (2.20) is satisfied.

To show that (2.21) is satisfied, we take $\widetilde{\mathbf{G}} \in X_h$, such that $(\widetilde{\mathbf{G}})^1_{e_k} = 1$ and all other components are zero. If e_k is an interior edge, (2.22) is satisfied automatically for any $\mathbf{v}$, since the discrete divergence operator does not depend on 1st moments on interior edges. If e_k is a boundary edge that belongs to the element E_i, using definition of the extended divergence operator, and noting that the quadrature $\mathcal{Q}_e$ is represented by the diagonal matrix $\mathbf{Q}_e$ (see formula (5.9) in Appendix A), we get

$$[\mathcal{D}^{\mathrm{h}}\widetilde{\mathbf{G}}, \mathbf{v}]_Q = -12|e_k|(\mathbf{v})^1_{e_k} = 0. \tag{2.25}$$

Thus (2.21) is satisfied. This completes the proof. □

2.4. Solution algorithm

To solve system (2.11) efficiently, we duplicate flux unknowns on interior mesh edges and use only the fluxes associated with element E in (2.17).

Let tilde in $(\widetilde{\mathbf{G}})^k_e$ denote a copy of $(\mathbf{G})^k_e$, $k = 0, 1$. For every interior edge e, we impose the trivial continuity conditions:

$$(\widetilde{\mathbf{G}})^k_e = (\mathbf{G})^k_e, \quad k = 0, 1. \tag{2.26}$$

To simplify notation, we write $\widetilde{\mathbf{G}}$ for the vector containing both $(\widetilde{\mathbf{G}})^k_e$ and $(\mathbf{G})^k_e$. The vector $\widetilde{\mathbf{F}}$ is defined similarly. The size of these new vectors is quadruple the number of interior edges plus twice the number of boundary edges. In addition, we use tilde for analogs of discrete operators and matrices introduced above. Then, solution of system (2.11) subject to continuity conditions (2.26) results in the following linear system [15, Chapter 16]:

$$\begin{bmatrix} \widetilde{\mathbf{M}}_X & \widetilde{\mathbf{B}}^{\mathrm{T}} & \mathbf{C}^{\mathrm{T}} \\ \widetilde{\mathbf{B}} & 0 & 0 \\ \mathbf{C} & 0 & 0 \end{bmatrix} \begin{bmatrix} \widetilde{\mathbf{F}} \\ \mathbf{u} \\ \boldsymbol{\lambda} \end{bmatrix} = \begin{bmatrix} 0 \\ \mathbf{q} \\ 0 \end{bmatrix}, \tag{2.27}$$

where $\boldsymbol{\lambda}$ is the vector of Lagrange multipliers, $\widetilde{\mathbf{B}} = \mathbf{M}_Q \widetilde{\mathcal{D}\mathcal{I}\mathcal{V}^{\mathrm{h}}}$, and the last block equation is the matrix representation of continuity conditions (2.26).

Observe that after rearranging rows and columns, the first 2×2 diagonal block in (2.27) is a block-diagonal matrix with as many blocks as there are mesh elements in $\mathcal{T}_h$. The size of each block is twice the number of mesh edges in E plus 1 (nine for quadrilaterals). Therefore, the vectors of flux and pressure unknowns in (2.27) can be readily eliminated resulting in a system for Lagrange multipliers with a sparse symmetric positive definite matrix. Efficient iterative methods, such as the preconditioned conjugate gradient method, can be used to solve this system. After that, the primary unknowns $\widetilde{\mathbf{F}}$ and $\mathbf{u}$ are calculated element-by-element.

3. The inner product in X_h

In this section, we show how to define the inner product (2.16) or, in other words, the appropriate quadrature rule $[\cdot,\cdot]_{X,E}$ on element E. The definition of an inner product implies that there exist a positive definite matrix $\mathbf{M}_E$, such that

$$[\mathbf{F},\mathbf{G}]_{X,E} = \mathbf{F}_E^{\mathrm{T}}\mathbf{M}_E\mathbf{G}_E, \tag{3.1}$$

where $\mathbf{F}_E$ (resp., $\mathbf{G}_E$) is a part of vector $\mathbf{F}$ (resp., $\mathbf{G}$) that includes only unknowns associated with element E. Let X_E^h denote the restriction of X^h to element E. For instance, for a quadrilateral element, $\mathbf{F}_E \in X_E^h$ is a vector of size 8.

We consider two methods for constructing $\mathbf{M}_E$. The first method extends the Kuznetsov–Repin approach [12,13] and requires a partition of the element E into triangles. It is useful for problems where the discrete solution $\mathbf{F}^h$ has to be interpolated in interior points of mesh elements. Moreover, this method can be easily extended to polyhedral meshes. The second method is algebraic and develops further ideas of [6]. It does *not* require an auxiliary triangular partition.

3.1. Method using an auxiliary triangular partition

This method consists of the following four steps, schematically illustrated on Fig. 3.

Step 1: (*Triangulation*). We partition element E into n_t, triangles $\Delta_1,\ldots,\Delta_{n_t}$. As shown in Fig. 2, there may be several ways of doing so. Note that a partition with fewer triangles requires less computational work.

On each interior edge, we define two *auxiliary* flux unknowns; namely, the 0th and 1st moments of the normal flux. These unknowns will be eliminated later. Let $\widetilde{X}_E^h$ be the new discrete space which includes original and auxiliary flux unknowns. For instance, $\widetilde{X}_E^h$ has dimension 14 for the partition shown in Fig. 2b and dimension 20 for the partition shown in Fig. 2c. Let $\widetilde{X}_\Delta^h$ be the restriction of $\widetilde{X}_E^h$ to the triangle Δ.

Step 2: (*Exact inner product on triangles*). Here we construct the inner product in space $\widetilde{X}_E^h$ from inner products in spaces $\widetilde{X}_{\Delta_i}^h$, $i=1,\ldots,n_t$. *Mimicking* the additivity property of integrals, we assume that

$$[\widetilde{\mathbf{F}}_E,\widetilde{\mathbf{G}}_E]_{\widetilde{X}_E^h} = \sum_{\Delta\in E}[\widetilde{\mathbf{F}}_\Delta,\widetilde{\mathbf{G}}_\Delta]_{\widetilde{X}_\Delta^h}$$

or, equivalently, that

$$\widetilde{\mathbf{F}}_E^{\mathrm{T}}\mathbf{M}_{E,\mathrm{huge}}\widetilde{\mathbf{G}}_E = \sum_{\Delta\in E}\widetilde{\mathbf{F}}_\Delta^{\mathrm{T}}\mathbf{M}_\Delta\widetilde{\mathbf{G}}_\Delta, \tag{3.2}$$

for any two vectors $\widetilde{\mathbf{F}}_E$ and $\widetilde{\mathbf{G}}_E$ in $\widetilde{X}_E^h$. The matrix $\mathbf{M}_{E,\mathrm{huge}}$ represents the inner product in space $\widetilde{X}_E^h$. Each matrix $\mathbf{M}_\Delta$ is a 6×6 symmetric positive definite matrix. We show that for the triangle Δ there exist only one matrix $\mathbf{M}_\Delta$ that exactly integrates the weighted product of two linear vector-functions.

A general linear vector-function $\vec{G}(x,y)$ has six parameters:

$$\vec{G}(x,y) = a_1\vec{\varphi}_1(x,y)+\cdots+a_6\vec{\varphi}_6(x,y) = \begin{bmatrix} a_1+a_3x+a_5y \\ a_2+a_4x+a_6y \end{bmatrix}. \tag{3.3}$$

For each triangle Δ, we define the matrix $\mathbf{M}_{\mathrm{coef}}$ as follows:

$$(\mathbf{M}_{\mathrm{coef}})_{ij} = \int_\Delta \vec{\varphi}_i^{\mathrm{T}}\cdot\overline{\mathbb{K}}_E^{-1}\vec{\varphi}_j\,\mathrm{d}x, \quad 1\leqslant i,j\leqslant 6. \tag{3.4}$$

This matrix is the quadrature rule in space Φ_Δ spanned by $\vec{\varphi}_1,\ldots,\vec{\varphi}_6$ over triangle Δ. Every linear function $\vec{G}$ can be uniquely represented by six moments on edges e_1, e_2 and e_3 of triangle Δ:

$$\int_{e_j}\vec{G}\cdot\vec{n}_{e_j}\,\mathrm{d}s \quad\text{and}\quad \int_{e_j}(\vec{G}\cdot\vec{n}_{e_j})s\,\mathrm{d}s, \quad j=1,2,3,$$

where s is the edge parametrization, $s\in[-1/2,1/2]$. Recall that these moments are our degrees of freedom. This implies that there exists a bijective (one-to-one) mapping $\mathbf{D}_\Delta$ from the space Φ_Δ to the space $\widetilde{X}_\Delta^h$. From linear algebra, we know that $\mathbf{D}_\Delta$ is the 6×6 matrix and its i-th column includes moments of $\vec{\varphi}_i\cdot\vec{n}_\Delta$ on the edges of Δ. Then, the aforementioned matrix $\mathbf{M}_\Delta$ is

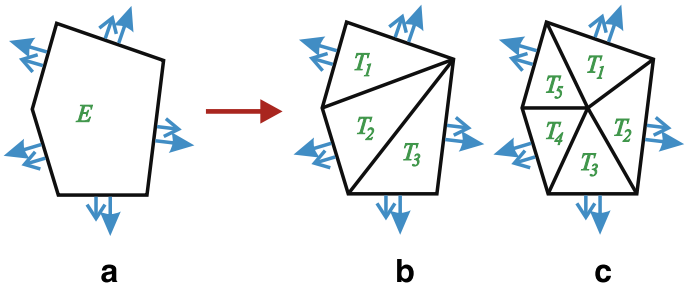

Fig. 2. Two sample ways (b) and (c) of triangulating a convex pentagon (a).

$$\mathbf{M}_{\Delta} = \mathbf{D}_{\Delta}^{-\mathrm{T}} \mathbf{M}_{\mathrm{coef}} \mathbf{D}_{\Delta}^{-1}. \tag{3.5}$$

According to (3.2), the matrix $\mathbf{M}_{E,\mathrm{huge}}$ is assembled from matrices $\mathbf{M}_{\Delta_i}$, $i = 1, \ldots, n_t$. Let us split the components of $\widetilde{\mathbf{G}} \in \widetilde{X}_E^h$ into three groups. The first group includes original (boundary) fluxes. The second and the third groups include the 0th and 1st moments on interior edges, respectively. After re-arranging rows and columns of $\mathbf{M}_{E,\mathrm{huge}}$ in accordance with this slitting, we get

$$\mathbf{M}_{E,\mathrm{huge}} = \left[\begin{array}{c|cc} \mathbf{M}_{bb} & \mathbf{M}_{ib}^0 & \mathbf{M}_{ib}^1 \\ \hline \mathbf{M}_{bi}^0 & \mathbf{M}_{ii}^{00} & \mathbf{M}_{ii}^{10} \\ \mathbf{M}_{bi}^1 & \mathbf{M}_{ii}^{01} & \mathbf{M}_{ii}^{11} \end{array}\right], \qquad \tilde{\mathbf{G}}_E = \left[\begin{array}{c} \mathbf{G}_E \\ \tilde{\mathbf{G}}_0 \\ \tilde{\mathbf{G}}_1 \end{array}\right]. \tag{3.6}$$

A similar partition holds for the vector $\widetilde{\mathbf{F}}_E$. For example, for the partition shown in Fig. 2b, $\mathbf{M}_{bb}$ is the 10×10 matrix, and $\mathbf{M}_{ii}^{00}$, $\mathbf{M}_{ii}^{11}$ are 2×2 matrices.

Step 3: (*Elimination of the 0th moments*). To eliminate the 0th moments on interior edges, we use the Kuznetsov–Repin method [12,13]. For a vector-function $\vec{G}$ that is linear on E, we get

$$\mathrm{div}(\vec{G})|_E = \mathrm{div}(\vec{G})|_{\Delta_i}, \quad i = 1, \ldots, n_t. \tag{3.7}$$

We *mimic* this property by insisting that

$$\mathcal{DIV}^{\mathrm{h}} \mathbf{G}_E = \mathcal{DIV}^{\mathrm{h}} \widetilde{\mathbf{G}}_{\Delta_i}, \quad i = 1, \ldots, n_t, \tag{3.8}$$

where the formula for the discrete divergence operator on triangle Δ_i is constructed similarly to (2.17). The discrete divergence operators involve only 0th moments. We rewrite linear relations (3.8) in the vector–matrix form:

$$\widetilde{\mathbf{G}}_0 = \mathbf{H} \mathbf{G}_E. \tag{3.9}$$

The matrix $\mathbf{H}$ is uniquely defined for some triangulations of E like that shown on the middle picture in Fig. 2. For other triangulations, like the right one in the same figure, this matrix may depend on a few free parameters.

Plugging (3.9) and a similar formula for $\widetilde{\mathbf{F}}_0$ into the inner product formula (3.2), we get:

$$\widetilde{\mathbf{G}}_E^{\mathrm{T}} \mathbf{M}_{E,\mathrm{huge}} \widetilde{\mathbf{F}}_E = \widehat{\mathbf{G}}_E^{\mathrm{T}} \mathbf{M}_{E,\mathrm{large}} \widehat{\mathbf{F}}_E, \tag{3.10}$$

where

$$\mathbf{M}_{E,\mathrm{large}} = \left[\begin{array}{c|c} \widehat{\mathbf{M}}_{bb} & \mathbf{M}_{ib}^1 \\ \hline \mathbf{M}_{bi}^1 & \mathbf{M}_{ii}^{11} \end{array}\right], \qquad \hat{\mathbf{F}}_E = \left[\begin{array}{c} \mathbf{F}_E \\ \tilde{\mathbf{F}}_1 \end{array}\right], \qquad \hat{\mathbf{G}}_E = \left[\begin{array}{c} \mathbf{G}_E \\ \tilde{\mathbf{G}}_1 \end{array}\right], \tag{3.11}$$

and

$$\widehat{\mathbf{M}}_{bb} = \mathbf{M}_{bb} + \mathbf{H}^{\mathrm{T}} \mathbf{M}_{ii}^{00} \mathbf{H} + \mathbf{M}_{ib}^0 \mathbf{H} + (\mathbf{M}_{ib}^0 \mathbf{H})^{\mathrm{T}}. \tag{3.12}$$

Step 4: (*Elimination of the 1st moments*). To eliminate the 1st moments on interior edges, we use the following observation. Let $\vec{F} = \mathbb{K} \nabla p$ and $\vec{G}$ be any non-zero vector-function such that

$$\begin{aligned} &\mathrm{div}\vec{G} = 0 \quad \text{in } E, \\ &\vec{G} \cdot \vec{n} = 0 \quad \text{on } \partial E. \end{aligned} \tag{3.13}$$

Then integration by parts gives

$$\int_E \vec{F} \cdot \mathbb{K}^{-1} \vec{G} \, \mathrm{d}x = -\int_E p(\mathrm{div}\vec{G}) \, \mathrm{d}x + \int_{\partial E} p(\vec{G} \cdot \vec{n}) \mathrm{d}x = 0. \tag{3.14}$$

We *mimic* property (3.14) by assuming that $\mathbf{F}_E$ is the discrete solution and its extension $\widehat{\mathbf{F}}_E$ satisfies:

$$\widehat{\mathbf{F}}_E^{\mathrm{T}} \mathbf{M}_{E,\mathrm{large}} \widehat{\mathbf{G}}_{\mathrm{int}} = 0 \quad \forall \widehat{\mathbf{G}}_{\mathrm{int}} = \left[\begin{array}{c} 0 \\ \tilde{\mathbf{G}}_1 \end{array}\right]. \tag{3.15}$$

Since $\tilde{\mathbf{G}}_1$ is arbitrary, condition (3.15) implies

$$\widetilde{\mathbf{F}}_1 = -(\mathbf{M}_{ii}^{11})^{-1} \mathbf{M}_{bi}^1 \mathbf{F}_E. \tag{3.16}$$

We impose the same restriction on vector $\widehat{\mathbf{G}}_E$ in (3.11). This immediately gives us

$$\widehat{\mathbf{G}}_E^{\mathrm{T}}\mathbf{M}_{E,\mathrm{large}}\widehat{\mathbf{F}}_E = \mathbf{G}_E^{\mathrm{T}}\mathbf{M}_{E,\mathrm{small}}\mathbf{F}_E,$$

where

$$\mathbf{M}_{E,\mathrm{small}} = \widehat{\mathbf{M}}_{bb} - \mathbf{M}_{ib}^{1}(\mathbf{M}_{ii}^{11})^{-1}\mathbf{M}_{bi}^{1}. \tag{3.17}$$

Our construction is completed by taking $\mathbf{M}_E \equiv \mathbf{M}_{E,\mathrm{small}}$.

To describe properties of matrix $\mathbf{M}_{E,\mathrm{small}}$, we define the space

$$\mathcal{F} = \overline{\mathbb{K}}_E\nabla(\mathcal{P}_2(E)),$$

where $\mathcal{P}_2(E)$ is the space of polynomials of order $\leqslant 2$. The dimension of space $\mathcal{F}$ is five and a general vector-function in $\mathcal{F}$ has the following form:

$$\vec{G} = a_1\vec{\psi}_1 + \cdots + a_5\vec{\psi}_5 = \overline{\mathbb{K}}\begin{bmatrix} a_1 + a_3x + a_4y \\ a_2 + a_4x + a_5y \end{bmatrix}. \tag{3.18}$$

Lemma 4. *Let $\vec{F}$ and $\vec{G}$ be two linear vector-functions from $\mathcal{F}$. Let $\mathbf{F}_E$ and $\mathbf{G}_E$ be their representations in X_E^h, i.e. $\mathbf{F}_E = (\vec{F})_E^I$ and $\mathbf{G}_E = (\vec{G})_E^I$. Then,*

$$\mathbf{F}_E^{\mathrm{T}}\mathbf{M}_{E,\mathrm{small}}\mathbf{G}_E = \int_E \vec{F}\cdot\overline{\mathbb{K}}_E^{-1}\vec{G}\,\mathrm{d}x.$$

Proof. We divide the proof into two parts. First, we show that the quadrature given by the matrix $\mathbf{M}_{E,\mathrm{large}}$ is exact for vector functions from $\mathcal{F}$. Then we show that the same property holds for the matrix $\mathbf{M}_{E,\mathrm{small}}$.

Part 1: (Properties of $\mathbf{M}_{E,\mathrm{large}}$). By construction, matrix $\mathbf{M}_{E,\mathrm{huge}}$ is the exact quadrature for the weighted L^2-product of any two vector-functions $\vec{F}_1$ and $\vec{G}_1$ that are piecewise linear on the triangular partition of E and have continuous normal components on interior mesh edges (i.e. $\vec{F},\vec{G}\in H_{\mathrm{div}}(E)$). In Step 3, we make assumption (3.8). From the definition of the divergence operator, we conclude that matrix $\mathbf{M}_{E,\ \mathrm{large}}$ is the exact quadrature for the weighted L^2-product of $\vec{F}_1$ and $\vec{G}_1$ that satisfy

$$\mathrm{div}\vec{F}_1 = \mathrm{const} \quad \text{and} \quad \mathrm{div}\vec{G}_1 = \mathrm{const}.$$

In particular, any $\vec{F}$ and $\vec{G}$ from $\mathcal{F}$ satisfy these requirements.

Part 2: (Properties of $\mathbf{M}_{E,\mathrm{small}}$). To prove that $\mathbf{M}_{E,\mathrm{small}}$ provides the exact quadrature rule for the weighted L^2-product of $\vec{F}$ and $\vec{G}$ from $\mathcal{F}$, it is sufficient to show that for all $u_2\in\mathcal{P}_2(E)$, the vector $\widehat{\mathbf{F}}_E$ defined by moments of $\overline{\mathbb{K}}_E\nabla u_2\cdot\vec{n}_E$ satisfies the condition (3.15). Let $\widehat{\mathbf{G}}_{\mathrm{int}}$ be of the form (3.15). Then there exists a piecewise linear $\vec{G}_1$ that satisfies (3.13) and such that

$$\widehat{\mathbf{G}}_{\mathrm{int}} = (\vec{G}_1)_E^I.$$

Indeed, on each triangle, $\vec{G}_1$ is uniquely defined by six moments on edges. Since $\vec{G}_1$ is piecewise linear, the continuity of $\vec{G}_1\cdot\vec{n}$ on interior mesh edges is enforced by construction. Thus,

$$\begin{aligned}\widehat{\mathbf{F}}_E^{\mathrm{T}}\mathbf{M}_{E,\mathrm{large}}\widehat{\mathbf{G}}_{\mathrm{int}} &= \int_E(\overline{\mathbb{K}}_E\nabla u_2)\cdot(\overline{\mathbb{K}}_E^{-1}\vec{G}_1)\mathrm{d}x\\ &= -\int_E u_2\mathrm{div}\vec{G}_1\,\mathrm{d}x + \int_{\partial E}u_2(\vec{G}_1\cdot\vec{n}_E)\mathrm{d}x = 0.\end{aligned}$$

This proves the assertion of the lemma. □

Remark 5. From the finite element viewpoint, the matrix $\mathbf{M}_{\mathcal{A}}$ from Step 2 is the mass matrix for the BDM_1 finite elements [3]. Also, formula (3.16) is used in the method of static condensation.

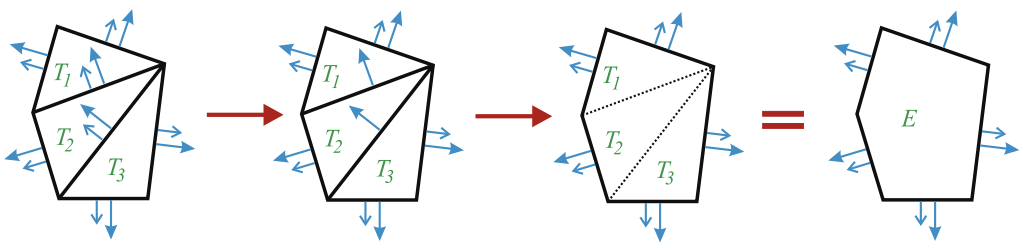

Fig. 3. Illustration of Steps 1–4 in construction of the matrix $\mathbf{M}_E$ for a pentagon.

3.2. Algebraic method

Let $\mathcal{L}_E$ and $\mathcal{L}_E^\perp$ be two proper subspaces of X_E^h such that any vector $\mathbf{G}_E \in X_E^h$ can be uniquely decomposed as follows:

$$\mathbf{G}_E = \mathbf{G}_1 + \mathbf{G}_\perp, \ \mathbf{G}_1 \in \mathcal{L}_E, \ \mathbf{G}_\perp \in \mathcal{L}_E^\perp.$$

We define $\mathcal{L}_E$ as the space of projections of all linear vector-functions from $\mathcal{F}$ into X_E^h. The other subspace is defined as the orthogonal complement to $\mathcal{L}_E$ with respect to the inner product induced by the matrix $\mathbf{M}_E$:

$$\begin{aligned} \mathcal{L}_E &= \{\mathbf{G}_1 \in X_E^h : \ \mathbf{G}_1 = (\vec{G})_E^I, \ \vec{G} \in \mathcal{F}\}, \\ \mathcal{L}_E^\perp &= \{\mathbf{G}_\perp \in X_E^h : \ \mathbf{G}_\perp^{\mathrm{T}} \mathbf{M}_E \mathbf{G}_1 = 0 \ \forall \mathbf{G}_1 \in \mathcal{L}_E\}. \end{aligned} \tag{3.19}$$

Let us choose a basis in X_E^h. We take five linearly independent vector-functions $\vec{\psi}_k$ from (3.18) to form five basis vectors in subspace $\mathcal{L}_E$:

$$\mathbf{V}_k = (\vec{\psi}_k)_E^I, \quad k = 1, \ldots, 5.$$

In general, we may pick an arbitrary basis in subspace $\mathcal{L}_E^\perp$. But before doing that, we need a more constructive definition of this subspace. Let $\vec{F} = \overline{\mathbb{K}}_E \nabla u_2$, where $u_2 \in \mathcal{P}_2(E)$. Then, the Gauss–Green formula for element E yields

$$\int_E \vec{F} \cdot \overline{\mathbb{K}}^{-1} \vec{G} \, \mathrm{d}x = -\int_E u_2 \mathrm{div} \vec{G} \, \mathrm{d}x + \int_{\partial E} u_2 \vec{G} \cdot \vec{n}_E \, \mathrm{d}x. \tag{3.20}$$

We *mimic* this formula as follows. Let, as before, $\mathbf{F}_E = (\vec{F})_E^I$ and $\mathbf{G}_E = (\vec{G})_E^I$. Furthermore, let $\mathcal{Q}_{\mathrm{left}}(\mathbf{F}_E, \mathbf{G}_E)$ be a quadrature rule for the integral in the left-hand side which is exact for any $\vec{F}, \vec{G} \in \mathcal{F}$. Let $\mathcal{Q}_{\mathrm{right}}(u_2, \mathbf{G})$ be a quadrature rule for the two integrals on the right-hand side of (3.20). We assume that it is exact for any $u_2 \in \mathcal{P}_2(E)$ and any linear vector-function $\vec{G} \in (\mathcal{P}_1(E))^2$. In addition, we assume that the matrix $\mathbf{M}_E$ can be used for $\mathcal{Q}_{\mathrm{left}}$,

$$\mathcal{Q}_{\mathrm{left}}(\mathbf{F}_E, \mathbf{G}_E) = \mathbf{F}_E^{\mathrm{T}} \mathbf{M}_E \mathbf{G}_E.$$

Finally, we assume that, for a given u_2, $\mathcal{Q}_{\mathrm{right}}(u_2, \mathbf{G}_E)$ is a linear functional on X_E^h and can be represented by the unique vector $\mathbf{U}_E \in X_E^h$ depending, of course, on u_2. We enforce

$$\mathcal{Q}_{\mathrm{left}}(\mathbf{F}_E, \mathbf{G}_E) = \mathcal{Q}_{\mathrm{right}}(u_2, \mathbf{G}_E) \tag{3.21}$$

or, equivalently,

$$\mathbf{F}_E^{\mathrm{T}} \mathbf{M}_E \mathbf{G}_E = \mathbf{U}_E^{\mathrm{T}} \mathbf{G}_E. \tag{3.22}$$

Derivation of the vector $\mathbf{U}_E$ is described in Appendix A. Choosing five linearly independent functions in $\mathcal{P}_2(E)$ (for example, x, y, x^2, xy and y^2), we generate five corresponding vectors $\mathbf{U}_{E,1}, \ldots, \mathbf{U}_{E,5}$. We show in Appendix A that $\mathcal{Q}_{\mathrm{right}}(1, \mathbf{G}_E) = 0$ for all $\mathbf{G}_E$ and therefore (3.21) is trivially satisfied. Then, the definition of subspace $\mathcal{L}_E^\perp$ becomes constructive:

$$\mathcal{L}_E^\perp = \{\mathbf{G}_\perp \in X_E^h : \ \mathbf{G}_\perp^{\mathrm{T}} \mathbf{U}_k = 0, \quad k = 1, \ldots, 5\}.$$

Let n_E be the number of edges in E, and $\mathbf{V}_6, \ldots, \mathbf{V}_{2n_E}$ be the orthonormal basis vectors in $\mathcal{L}_E^\perp$:

$$\mathbf{V}_k^{\mathrm{T}} \mathbf{V}_l = \delta_{kl}, \quad 6 \leqslant k, \quad l \leqslant 2n_E.$$

Let $\mathbf{D}_E$ be the $2n_E \times 2n_E$ matrix whose i-th columns is vector $\mathbf{V}_i$. With abuse of notations, we define a 5×5 symmetric positive definite matrix $\mathbf{M}_{\mathrm{coef}}$:

$$(\mathbf{M}_{\mathrm{coef}})_{ij} = \int_E \vec{\psi}_i \cdot \overline{\mathbb{K}}_E^{-1} \vec{\psi}_j \, \mathrm{d}x.$$

Inspired by Lemma 4 and our previous research on MFD methods [6,2], we define the matrix $\mathbf{M}_E$ as follows:

$$\mathbf{M}_E = \mathbf{D}_E^{-\mathrm{T}} \begin{bmatrix} \mathbf{M}_{\mathrm{coef}} & 0 \\ 0 & |E| \mathbf{A}_E \end{bmatrix} \mathbf{D}_E^{-1}, \tag{3.23}$$

where $\mathbf{A}_E$ is an arbitrary symmetric positive-definite matrix. From practical viewpoint, we may use the properly scaled identity matrix:

$$\mathbf{A}_E = a_E \mathbf{I}_E, \quad a_E = \mathrm{trace}(\overline{\mathbb{K}}_E).$$

Remark 6. The solution algorithm described in Section 2.4 uses only inverse of the matrix $\mathbf{M}_E$. According to (3.23), calculation of $\mathbf{M}_E^{-1}$ requires to invert only matrix $\mathbf{M}_{\mathrm{coef}}$ of size 5. This makes the algebraic approach more attractive for practical implementation than the approach described in the previous section.

3.3. Remarks on the low-order MFD method

The inner product matrix developed in [6] for the low-order MFD method can be also written in form (3.23). For completeness of the presentation, we provide a few additional details. We shall use superscript '(0)' to stress that notations now are related to the low-order MFD method.

The space $\mathcal{F}^{(0)} = \overline{\mathbb{K}}_E \nabla(\mathcal{P}_1(E))$ is based on gradients of linear functions and, therefore, has dimension two. The two linearly independent vectors are

$$\vec{\psi}_1 = \overline{\mathbb{K}}_E \nabla x \quad \text{and} \quad \vec{\psi}_2 = \overline{\mathbb{K}}_E \nabla y.$$

Thus, the matrix $\mathbf{M}^{(0)}_{\text{coef}} = \overline{\mathbb{K}}_E$.

These similarities imply that the analysis performed in [4] for the low-order MFD method can be extended to the high-order method to rigorously prove the second-order convergence estimates for both scalar and vector variables in the high-order MFD methods. This will be the topic for future research.

4. Numerical experiments

We made a number of numerical experiments to verify the rate of convergence of the high-order MFD method and to compare it with the low-order MFD method. The comparison has been done on sequences of randomly perturbed quadrilateral and smooth polygonal median meshes.

Let $(u, \vec{F})$ be the continuum solution to the problem (2.3) and $(\mathbf{u}_h, \mathbf{F}_h)$ be the solution to the corresponding discrete problem. We define the errors as follows:

$$\begin{aligned} \varepsilon_u &= |||(u)^I - \mathbf{u}_h|||_Q \equiv [(u)^I - \mathbf{u}_h, (u)^I - \mathbf{u}_h]_Q^{1/2}, \\ \varepsilon_F &= |||(\vec{F})^I - \mathbf{F}_h|||_X \equiv [(\vec{F})^I - \mathbf{F}_h, (\vec{F})^I - \mathbf{F}_h]_X^{1/2}. \end{aligned} \tag{4.1}$$

A randomly perturbed mesh (see the left picture in Fig. 4) is built from a square mesh with mesh size $h = 1/n$ by relocating each interior mesh node p to a random position inside a square box $\mathcal{B}(p)$. The box is centered at p, its sides are aligned with the coordinate axis, and its size is $h/2$. Convergence analysis on the sequence of randomly perturbed meshes is the challenging test for any discretization method.

A polygonal median mesh (see Fig. 4b) is built in two steps. First, we generate the Voronoi tessellation for the set of points $(x_{i,j}, y_{i,j})$ given by

$$\begin{aligned} x_{i,j} &= \xi_i + 0.1 \sin(2\pi\xi_i)\sin(2\pi\eta_j), \qquad i = 0, \ldots, n, \\ y_{i,j} &= \eta_j + 0.1 \sin(2\pi\xi_i)\sin(2\pi\eta_j), \qquad j = 0, \ldots, n, \end{aligned}$$

where $\xi_i = ih$, $\eta_j = jh$ and $h = 1/n$. Second, we move each interior mesh node p to the center of mass of a triangle formed by the centers of three Voronoi cells sharing p.

Experiment 1: (*Constant tensor*). We consider the problem (2.1) in the unit square $[0,1]^2$ with $\mathbb{K} = \mathbb{I}$ and the exact solution

$$u(x,y) = \sin(\pi x)\sin(\pi y). \tag{4.2}$$

The results of calculations on the sequence of randomly perturbed quadrilateral meshes are shown in Fig. 5. Both low-order and high-order MFD methods exhibit the second-order convergence rate for u in the mesh-dependent L^2-norm (4.1). The

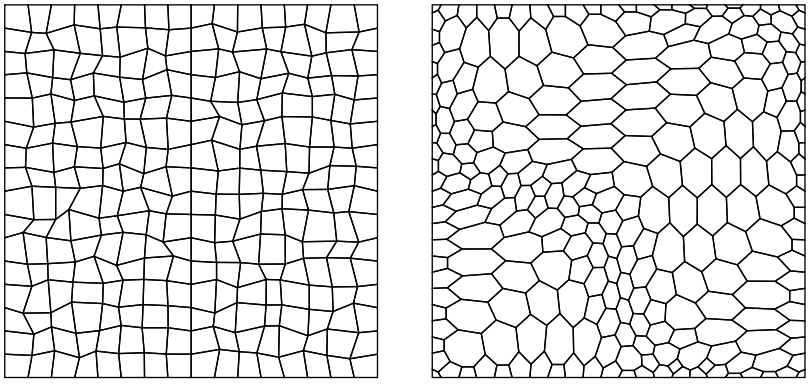

Fig. 4. Sample meshes from two sequences. Picture (a) shows a randomly perturbed quadrilateral mesh. Picture (b) shows a polygonal median mesh.

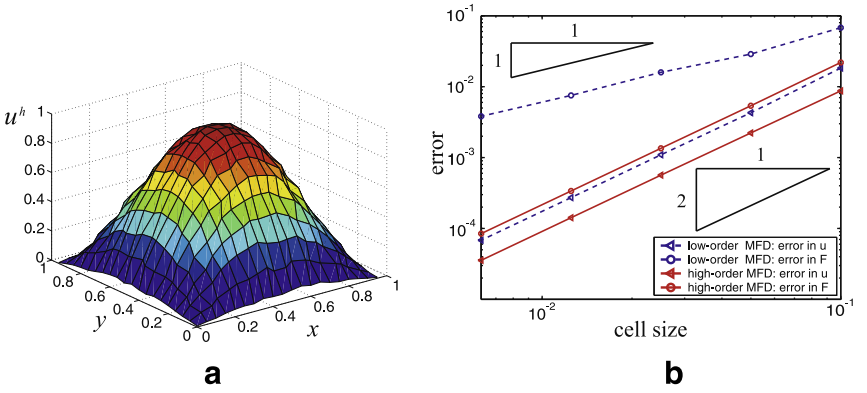

Fig. 5. Picture (a) shows the discrete solution for the problem in Experiment 1 on the 20×20 randomly perturbed quadrilateral mesh. Picture (b) shows convergence rates for the low-order and high-order MFD methods.

low-order MFD method shows only the first-order convergence rate for the flux $\vec{F}$ in the mesh-dependent norm, while in the high-order MFD method the convergence rate is second-order.

Experiment 2: (*Discontinuous tensor*). We consider again the problem (2.1) in the unit square $[0,1]^2$ with the piecewise constant tensor $\mathbb{K}$,

$$\mathbb{K}(x,y) = \begin{cases} \alpha = 10^{-3} & \text{for } x < 0.5, \\ 1 & \text{for } x > 0.5 \end{cases} \tag{4.3}$$

and the exact solution

$$u(x,y) = \begin{cases} y(y-1)x^2 & \text{for } x < 0.5, \\ y(1-y)(1-x)(\alpha - x(1+2\alpha)) & \text{for } x > 0.5. \end{cases} \tag{4.4}$$

The results of calculations on the sequence of randomly perturbed quadrilateral meshes are shown in Fig. 6. As in the precious example, the high-order MFD method is second-order accurate for both u and $\vec{F}$. Both methods are second-order accurate for u; however, the actual error is about six times smaller in the high-order MFD method.

Experiment 3: (*Full tensor*). We consider once more the problem (2.1) in the unit square $[0,1]^2$, first with the full isotropic tensor $\mathbb{K}_1$ and then with the full anisotropic tensor $\mathbb{K}_2$:

$$\mathbb{K}_1 = \begin{bmatrix} 10 & 3 \\ 3 & 10 \end{bmatrix}, \quad \mathbb{K}_2 = \begin{bmatrix} 10 & 3 \\ 3 & 1 \end{bmatrix}.$$

Let (4.2) be the exact solution. The eigenvalues of $\mathbb{K}_2$ are approximately 0.092 and 10.91, which implies that $\mathbb{K}_2$ is the strongly anisotropic tensor.

The results of calculations on the sequence of polygonal median meshes are shown in Fig. 7. We observe some super-convergence (1.5–1.6) of the flux $\vec{F}$ in the low-order MFD method. This implies that the polygonal meshes have underlying smoothness. The high-order MFD method is again second-order accurate for both u and $\vec{F}$.

Experiment 4: (*Efficacy*). We compare the low-order and high-order MFD methods for the problem with the discontinuous coefficient. Efficacy of the method (accuracy versus cost) depends on many factors including optimality of the chosen linear

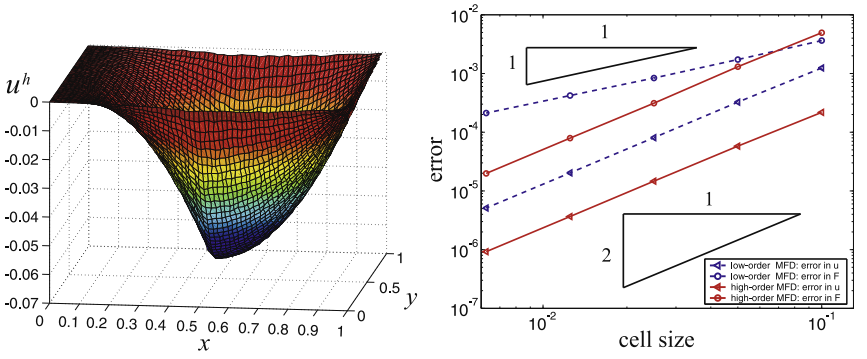

Fig. 6. The left picture shows the discrete solution on the 64×64 randomly perturbed quadrilateral mesh. The right picture shows convergence rates for the low-order and high-order MFD methods for the problem in Experiment 2.

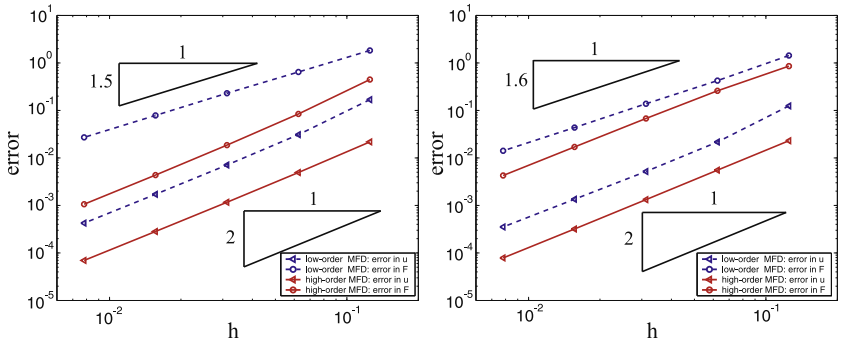

Fig. 7. Convergence rates for the low-order and high-order MFD methods on polygonal median meshes for the problem in Experiment 3. The left picture shows convergence rates for the constant full isotropic tensor $\mathbb{K}_1$. The right picture shows convergence rates for the full anisotropic tensor $\mathbb{K}_2$.

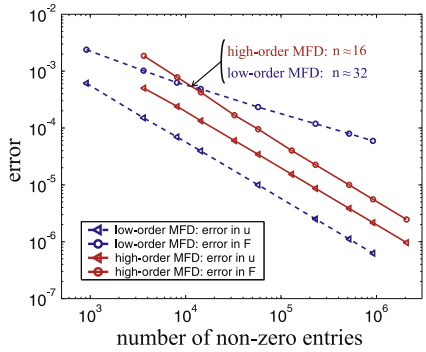

Fig. 8. Accuracy of the low-order (dashed lines) and high-order (solid lines) MFD methods versus the number of non-zero entries in the matrix employed in the linear solver. The circles and triangles correspond to the scalar and vector variables, respectively.

solver. Optimal linear solvers, such as the algebraic multigrid solver, may be adjusted to high-order discretizations [16], which makes a fair comparison a non-trivial task. Here, we assume that complexity of a linear solver is proportional to the number of non-zero entries in the matrix. In our case, this is the matrix of a linear system for the Lagrange multipliers (see Section 2). The graphs for the scalar variable u in Fig. 8 do not intersect since both methods are second-order accurate for this variable. However, graphs for the flux variable do intersect. This implies that the high-order MFD method becomes more efficient than the low-order MFD on relatively coarse meshes of $n \times n$ cells ($n \geqslant 16$).

5. Conclusion

We developed new high-order mimetic finite difference methods which are second-order accurate for both scalar variable u and its flux $\vec{F}$. The first method is based on partition of each polygonal cell into triangles. The second one uses only the normals to polygon edges, length of edges, and quadrature rules for edge integrals. The second method results in a family of discretizations with equivalent properties. Both methods were developed in two-dimensions. Their extension to three dimensions will be the topic for future research.

Acknowledgments

This work was carried out under the auspices of the National Nuclear Security Administration of the US Department of Energy at Los Alamos National Laboratory under Contract No. DE-AC52-06NA25396 and the DOE Office of Science Advanced Scientific Computing Research (ASCR) Program in Applied Mathematics Research. The work of Vitaliy Gyrya was partially supported by the National Science Foundation, grant number DMS-0708324.

Appendix A

Here we explain how to construct the quadrature rule $\mathcal{Q}_{\text{right}}(u_2, \mathbf{G}_E)$, $\mathbf{G}_E = (\vec{G})^I_E$, for the right-hand side of (3.20) which is exact for any quadratic $u_2 \in \mathcal{P}_2(E)$ and linear $\vec{G} \in (\mathcal{P}_1(E))^2$.

Let ϕ_i, $i = 1, \ldots, 5$, be the functions from $\mathcal{P}_2(E)$ such that $\nabla\phi_i = \vec{\psi}_i$, where $\vec{\psi}_i$ is defined in (3.18). Then, any $u_2 \in \mathcal{P}_2(E)$ can be represented as follows:

$$u_2 = b_0 + b_1\phi_1 + \cdots + b_5\phi_5.$$

First, we consider the case $b_0 = 0$. Let $\mathbf{b}$ be the vector in $\mathcal{R}^5$, $\mathbf{b} = (b_1, \ldots, b_5)^{\mathrm{T}}$. The first term in $\mathcal{Q}_{\mathrm{right}}$ comes from the area integral. Since $\mathrm{div}\vec{G}$ is constant, we apply the following exact quadrature:

$$\int_E u_2 \mathrm{div}\vec{G}\,\mathrm{d}x = (\mathcal{DIV}_{\mathrm{E}}^{\mathrm{h}}\mathbf{G}_E)\mathbf{b}^{\mathrm{T}}\mathbf{a} \equiv \mathbf{b}^{\mathrm{T}}\mathbf{Q}_1\mathbf{G}_E, \tag{5.5}$$

where $\mathcal{DIV}_{\mathrm{E}}^{\mathrm{h}}$ is a $1 \times 2n_E$ matrix, a part of the discrete divergence matrix $\mathcal{DIV}^{\mathrm{h}}$, $\mathbf{Q}_1$ is the $5 \times 2n_E$ matrix, and

$$\mathbf{a} = (a_1, \ldots, a_5)^{\mathrm{T}}, \quad a_i = \int_E \phi_i\,\mathrm{d}x.$$

Note that integration over element E is easily reduced to integration over ∂E using the divergence theorem.

The second term in $\mathcal{Q}_{\mathrm{right}}$ comes from the boundary integral. Formally, we can write

$$\int_{\partial E} u_2(\vec{G}\cdot\vec{n}_E)\,\mathrm{d}x = \mathbf{b}^{\mathrm{T}}\mathbf{Q}_2\mathbf{G}_E, \quad \mathbf{Q}_2 = [\mathbf{Q}_{2,1}, \ldots, \mathbf{Q}_{2,n_E}], \tag{5.6}$$

where $\mathbf{Q}_2$ is the $5 \times 2n_E$ matrix and the 5×2 matrix $\mathbf{Q}_{2,j}$ corresponds to the j-th edge of E. Let us consider the first edge, e_1, and denote the i-th row of $\mathcal{Q}_{2,1}$ by $\mathcal{Q}_{2,1}^{(i)}$. Then

$$\phi_i|_{e_1} = c_1 + c_2 s + c_3 s^2,$$

where s is the parametrization of edge e_1, $s \in [-1/2, 1/2]$. Let $X_{e_1}^h$ be restriction of X_E^h to edge E, and $\mathbf{T}_1$ be a mapping from $X_{e_1}^h$ to $\mathcal{P}_1([-1/2, 1/2])$,

$$\mathbf{T}_1 = \begin{bmatrix} 1 & 0 \\ 0 & 12 \end{bmatrix}.$$

Note that

$$\int_{e_1} \phi_i(d_1 + d_2 s)\,\mathrm{d}x = \mathbf{c}_i^{\mathrm{T}}\mathbf{R}\mathbf{d}, \tag{5.7}$$

where

$$\mathbf{c}_i = (c_{i1}, c_{i2}, c_{i3})^{\mathrm{T}}, \quad \mathbf{d} = (d_1, d_2)^{\mathrm{T}} \quad \text{and} \quad \mathbf{R} = |e_1| \begin{bmatrix} 1 & 0 \\ 0 & 1/12 \\ 1/12 & 0 \end{bmatrix}.$$

Thus, $\mathbf{Q}_{2,1}^{(i)} = \mathbf{c}_i^{\mathrm{T}}\mathbf{R}\mathbf{T}_1$. The other edges of E are treated in the same way. Finally,

$$\mathcal{Q}_{\mathrm{right}}(u_2, \mathbf{G}_E) = \mathbf{b}^{\mathrm{T}}(\mathbf{Q}_2 - \mathbf{Q}_1)\mathbf{G}_E \tag{5.8}$$

and the vectors $\mathbf{U}_E$ in (3.22) are the rows of matrix $\mathbf{Q}_2 - \mathbf{Q}_1$.

Now, we consider the case $u_2 = b_0$. Using the above notations, we get that $\mathbf{a} = |E|$ and $\mathbf{Q}_{2,1} = |e_1|[1\ 0]$. The definition of the divergence implies that $\mathbf{Q}_2 = \mathbf{Q}_1$, i.e. $\mathcal{Q}_{\mathrm{right}}(1, \mathbf{G}_E) = 0$ for any $\mathbf{G}_E$.

The argument similar to that used in derivation of (5.8) can be used to get the quadrature rule for the edge integral in (2.15):

$$\mathcal{Q}_e(\mathbf{u}, \mathbf{v}) = \mathbf{u}_e^{\mathrm{T}}\mathbf{Q}_e\mathbf{v}_e,$$

where $\mathbf{u}_e, \mathbf{v}_e$ are restriction of $\mathbf{u}, \mathbf{v} \in Q^h$ to the edge e, and

$$\mathbf{Q}_e = |e|\mathbf{T}_1^{\mathrm{T}} \begin{bmatrix} 1 & 0 \\ 0 & 1/12 \end{bmatrix} \mathbf{T}_1 = |e| \begin{bmatrix} 1 & 0 \\ 0 & 12 \end{bmatrix}. \tag{5.9}$$

References

[1] J.E. Aarnes, S. Krogstad, K.-A. Lie, Multiscale mixed/mimetic methods on corner-point grids. Comput. Geosci. Special Issue on Multiscale Methods (2007), doi:10.1007/s10596-007-9072-8.

[2] F. Brezzi, A. Buffa, K. Lipnikov, Mimetic finite differences for elliptic problems, Los Alamos Report LAUR 07-8140, M2AN: Math. Model. Numer. Anal. (2007), submitted for publication.

[3] F. Brezzi, M. Fortin, Mixed and Hybrid Finite Element Methods, Springer-Verlag, New York, 1991.

[4] F. Brezzi, K. Lipnikov, M. Shashkov, Convergence of mimetic finite difference method for diffusion problems on polyhedral meshes, SIAM J. Numer. Anal. 43 (5) (2005) 1872–1896.

[5] F. Brezzi, K. Lipnikov, M. Shashkov, V. Simoncini, A new discretization methodology for diffusion problems on generalized polyhedral meshes, Comput. Methods Appl. Mech. Eng. 196 (2007) 3682–3692.

[6] F. Brezzi, K. Lipnikov, V. Simoncini, A family of mimetic finite difference methods on polygonal and polyhedral meshes, Math. Mod. Meth. Appl. Sci. 15 (10) (2005) 1533–1552.

[7] J. Campbell, M. Shashkov, A tensor artificial viscosity using a mimetic finite difference algorithm, J. Comput. Phys. 172 (2001) 739–765.
[8] J.E. Castillo, J.M. Hyman, M.J. Shashkov, S. Steinberg, High-order mimetic finite difference methods on nonuniform grids, in: A.V. Ilin, L.R. Scott (Eds.), Special Issue of Houston Journal of Mathematics, 1995, pp. 347–361.
[9] J.E. Castilloi, R.D. Grone, A matrix analysis approach to higher-order approximations for divergence and gradients satisfying a global conservation law, SIAM J. Matrix Anal. Appl. 25 (1) (2003) 128–142.
[10] P.G. Ciarlet, The Finite Element Method for Elliptic Problems, North-Holland, New York, 1978.
[11] J. Hyman, M. Shashkov, Mimetic discretizations for Maxwell's equations and the equations of magnetic diffusion, Progr. Electromagn. Res. 32 (2001) 89–121.
[12] Yu. Kuznetsov, S. Repin, New mixed finite element method on polygonal and polyhedral meshes, Russ. J. Numer. Anal. Math. Model. 18 (3) (2003) 261–278.
[13] Yu. Kuznetsov, S. Repin, Convergence analysis and error estimates for mixed finite element method on distorted meshes, J. Numer. Math. 13 (1) (2005) 33–51.
[14] L. Margolin, M. Shashkov, P. Smolarkiewicz, A discrete operator calculus for finite difference approximations, Comput. Meth. Appl. Mech. Eng. 187 (2000) 365–383.
[15] J. Nocedal, S. Wright, Numerical Optimization, Springer, Berlin, Heidelberg, New York, 1999.
[16] L. Olson, Algebraic multigrid preconditioning of high-order spectral elements for elliptic problems on a simplicial mesh, SIAM J. Sci. Comput. 29 (5) (2007) 2189–2209.
[17] J.B. Perot, V. Subramanian, Higher-order mimetic methods for unstructured meshes, J. Comput. Phys. 219 (1) (2006) 68–85.
[18] R. Rieben, Mixed finite element methods for Lagrangian hydrodynamics, Technical Report, Lawrence Livermore National Laboratory, 2007. UCRL-PRES-2312264.